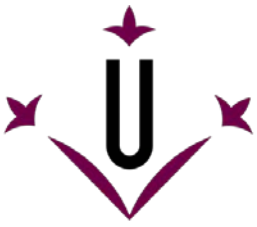

Effect of polymer coating composition on the aggregation rates of Ag nanoparticles in NaCl solutions and seawaters

Pablo Lodeiro[a,b*], Eric P. Achterberg[a,b], Carlos Rey-Castro[c] and Mohammad S. El-Shahawi[d,1]

[a]Ocean and Earth Science, University of Southampton, National Oceanography Centre, European Way, SO14 3ZH Southampton, UK.

[b]GEOMAR Helmholtz Centre for Ocean Research Kiel, Wischhofstraße 1-3, 24148 Kiel, Germany

[c]Departament de Química, Universitat de Lleida and AGROTECNIO, Rovira Roure 191, 25198, Lleida, Spain

[c]Departament de Química, Universitat de Lleida and AGROTECNIO, Rovira Roure 191, 25198, Lleida, Spain

[d]Department of Chemistry, Faculty of Science, King Abdulaziz University, P. O. Box 80203, Jeddah 21589, Kingdom of Saudi Arabia (on sabbatical leave)

[1]On sabbatical leave from the Department of Chemistry, Faculty of Science, Damietta University, Damietta, Egypt.

*Corresponding Author: plodeiro@geomar.de

Abstract

The aggregation behaviour of polymer-coated silver nanoparticles (AgNPs) was characterized in NaCl solutions, and in two seawaters of different salinities and dissolved organic matter (DOM) contents. Representative organic coatings i.e. tannic acid (TA), alginic acid (ALG), two gum Arabic samples (GAL and GAH), branched polyethylenimine (BPEI), and non-ionic surfactants (reference material NM-300K) were selected to cover a wide range of zeta-potentials. The stability in NaCl solutions, as determined from the rate of variation in hydrodynamic size within a timeframe of one hour, followed the order BPEI >> NM-300K ≈ GAL >> ALG ≈ TA >>GAH. In the seawater samples the order was NM-300K ≈ GAL >> ALG > GAH > TA ≈ BPEI, and only TA, GAL and NM-300K batches behaved as expected from the NaCl experiments. Remarkably, the BPEI sample showed the largest aggregation rate in the seawater sample with the highest DOM concentration (277 µM C). The GAH sample displayed a non-monotonic variation in aggregation rate with NaCl concentration, apparently due to concomitant precipitation of AgCl. The results indicate that non-electrostatic stabilization mechanisms and DOM-coating interactions are important for the prediction of stability and persistence of polymer-coated AgNPs in seawater.

Keywords: Silver nanoparticles; aggregation; seawater; organic coatings; NaCl media.

1. Introduction

Silver nanoparticles (AgNPs) have been extensively studied because of their widespread use in consumer products (McGillicuddy et al., 2017). However, the impact of AgNPs on the natural environment is not yet fully understood. There are still uncertainties with respect to the behaviour of specific nanoparticles (NPs) upon discharge into natural waters (Bour et al., 2015; Pokhrel et al., 2014; Sharma, 2013). Aggregation studies are therefore critical to enhance our mechanistic and quantitative process understanding and will allow us to model the behaviour and fate of NPs in the environment, including quantification of their risks (Afshinnia et al., 2017; Chekli et al., 2015; Lodeiro et al., 2016). Mechanistic mathematical models have been developed in recent years for the assessment of projected environmental NP concentrations, mostly based on conceptual variations of the population balance equation. These models include homo- and heteroaggregation rate expressions (based on the Smoluchowski equation) with variable attachment efficiencies, gravitational settling rates coupled or not to fractal models of the aggregate structure and possible breakage of agglomerates (Arvidsson et al., 2011; Dale et al., 2017; Gregory, 2005; Quik et al., 2014; Scheringer et al., 2014). Although there is still a large uncertainty in many of the required physicochemical input parameters, several simulation scenarios have highlighted the importance of heteroaggregation rates with natural particulate matter (Praetorius et al., 2012). Furthermore, in absence of natural colloids, the scenarios have indicated the predominance of the perikinetic aggregation mechanism (Handy et al., 2008) (caused by Brownian motion) and the extreme sensitivity to collision efficiencies (Arvidsson et al., 2011). The values

of the effective aggregation rates and fractal structure parameters could, in principle, be obtained in the laboratory from aggregation experiments performed in synthetic solutions, as explained below. Several important contributions have been recently presented on the effect of natural dissolved organic matter (DOM) on the stability behaviour of NPs in samples representative of environmental conditions (Afshinnia et al., 2018; Baalousha et al., 2013a; Ellis et al., 2016) However, the specific role of the organic coating composition in the interactions of NPs with DOM still remains largely unknown.

The use of appropriate coatings is required to preserve the physical and chemical stability of NPs. Polymer-coated AgNPs constitute a representative example of extensively used NPs in commercial products (e.g. food packaging, cosmetics, clothing, etc.) (Chernousova and Epple, 2013; Nowack et al., 2011). The investigation of reference nanomaterials, e.g. NM-300K AgNPs, is also relevant due to their use in hazard identification measurements, testing studies, and safety evaluation of NPs (Tantra et al., 2016). Thus, we studied here a characteristic range of manufactured NPs (both commercial and laboratory samples) that constitute an important target group for aggregation kinetic studies.

Characterization of the aggregation behaviour of engineered nanoparticles in synthetic electrolyte solutions is a typical physicochemical endpoint in the assessment of their fate and behaviour in natural waters. This approach is hindered by the representativeness of synthetic solution compositions with respect to real samples, as well as the complexity of interactions between NP coatings and constituents of the aqueous matrix. Chloride ions are present in

most natural waters and at high concentrations in seawaters (0.56 M at salinity 35). Thus, we used NaCl as a key reactive electrolyte to study AgNP aggregation. The results were compared to those obtained in seawaters to assess whether these simple solutions are representative of natural waters in terms of AgNP aggregation behaviour.

Here we study the aggregation kinetics of five different polymer-coated AgNPs by dynamic light scattering (DLS) at increasing NaCl concentrations. The DLS technique allows the calculation of the z-average hydrodynamic diameter (*d*) and polydispersity index (Pdi) of the NPs, based on measurements of light scattered by NPs in solution (Brar and Verma, 2011). Accordingly, the size increase of AgNPs in aqueous media can be monitored over time using DLS (Baalousha et al., 2013b; Metreveli et al., 2016). In addition, we used two natural seawaters with different salinities and organic matter contents to investigate AgNPs behaviour in marine waters by DLS. We found significant differences in the aggregation behaviour of the AgNPs between NaCl and the seawater solutions, reflecting the additional complexities in natural waters.

Unfortunately, the estimated low environmental NP concentrations (ppt range) (Massarsky et al., 2014) cannot be measured using DLS. Therefore, the limits of extrapolation of the obtained results (ppm range concentrations) to dilute systems must be considered cautiously. Alternative simple methods, such as UV-visible spectrophotometry using long path cells, allow a considerable reduction in the detection limit of NPs in seawaters (Lodeiro et al., 2017), although this method is likely more sensitive to Ag oxidation than DLS.

The aggregation kinetic studies in the present work were focused on the onset of aggregation when only small aggregates (<250 nm) are formed. Precipitation or sedimentation phenomena were not taken into account, and only Brownian aggregation was considered as a NP destabilization mechanism. The expected lifetime of AgNPs dispersions in the upper surface layers, right after their discharge into seawater, is assumed to depend on the role of the organic coatings on the short-term aggregation behaviour of the NPs. We are aware of the important limits of this approach regarding long-term behaviour and fate of AgNP aggregates. Nevertheless, the limitations of the DLS technique and the difficulties of simulating environmentally realistic hydrodynamic conditions in the lab (only Brownian aggregates are relevant in the quiescent conditions of DLS cuvettes) hinder the study of relatively large aggregates, which are also subjected to a vertical component of movement due to the combination of drag, buoyancy and gravitational forces. Settling of particles will therefore be relevant for longer times than those studied here and for subsurface water layers.

In summary, the main goals of this study are: First, to characterize the aggregation kinetics of AgNPs with six different organic coatings covering a wide range of molecular weights and electrostatic properties (neutral, positively and negatively charged) as a function of NaCl concentration. For this purpose, the z-averaged collision efficiencies, critical coagulation concentrations, and aggregation rate constants were derived from time-resolved DLS experiments. Second, to test the aggregation behaviour of the same NP batches in natural seawater samples of different salinities and DOM contents; and, finally, to compare the stability in seawater with that in NaCl

125 solutions of similar ionic strength. This will permit evaluation of the
126 representativeness of NaCl as a model background electrolyte for the
127 prediction of fate and behaviour in seawaters, and to obtain qualitative
128 conclusions on the role of the coating composition and the presence of natural
129 DOM.
130
131 **2. Material and methods**
132 **2.1 Materials**
133 The chemicals used throughout the experiments were purchased from Sigma-
134 Aldrich (Dorset, UK) and Fisher Scientific (Leicestershire, UK). High-purity
135 water (Millipore, Watford, UK) with a resistivity of 18.2 MΩ cm^{-1} was used. The
136 natural surface seawater samples were collected in a Baltic fjord located in
137 northwest Germany (54°22.1' N 10º11.7' E) and A Coruña Bay (43º21.8' N
138 8º23.4' W) in northwest Spain. The samples were filtered through a 0.45 µm
139 pore size polycarbonate membrane filter (Whatman Int. Ltd) and stored in acid
140 cleaned low-density polyethylene bottles (Nalgene) before use. The
141 composition of the seawater samples is presented in Table S2.
142 AgNPs coated with alginate (ALG) and gum Arabic (GAH and GAL, where L
143 denotes low Ag^+ and H high Ag^+ residual content after dialysis purification)
144 were synthesized by chemical reduction of silver nitrate (see (Lodeiro et al.,
145 2016) for details). In addition, the silver reference nanomaterial NM-300K
146 (obtained from Fraunhofer Institute for Molecular Biology and Applied
147 Ecology, Germany), AgNPs coated with tannic acid (TA) and branched
148 Polyethylenimine (BPEI) (BioPure, nanoComposix Inc) were also studied.
149 NM-300K consists of colloidal spherical AgNPs. The stabilizing capping agent

for NM-300K NPs is an aqueous mixture of non-ionic surfactants comprising 4% (w/w) polyoxyethylene glycerol trioleate and 4% (w/w) polyoxyethylene sorbitan monolaurate (Tween-20) (Klein et al., 2011).

2.2 Dynamic light scattering measurements

The z-average hydrodynamic diameter and zeta-potential values were measured using a Zetasizer (Nano-ZS, Malvern instruments Ltd) with a He-Ne laser (633 nm). The scattered light from the DLS measurements was collected and detected at an angle of 173º. The analysis of the obtained autocorrelation function using Malvern software (cumulants method) provided the intensity-weighted particle size distributions, measured as the z-average hydrodynamic diameter (*d*). An indication of the width of the size distribution was also acquired using the polydispersity index (Pdi) from the DLS data. The viscosity and refractive index values used in the Malvern software are shown in Table S3. Moreover, electrophoretic mobility measurements were transformed to zeta-potentials using Henry's equation under the Smoluchowski's approximation using the software provided by the Malvern instrument (Ohshima, 2006). At least two replicates for each experiment were measured. In the first replicate the attenuation factor and laser position were set to automatic on the equipment, while for the second one and successive replicates, the manual option using the previously obtained optimal parameters was selected. In this way, more data at the on-set of the aggregation process could be obtained (at least 15-20 s are needed to obtain a value for *d*). The raw *d versus t* curves used for the CCC calculations (Figure 1) were fitted to a polynomial spline function. A new set of values was

interpolated at a fixed time step of 5 seconds, while the kinetic aggregation constants were calculated using the raw data obtained from the experiments. The pH of AgNP solutions was adjusted to pH 8.0 ± 0.2 by addition of appropriate quantities of NaOH and measured using a ThermoScientific pH meter Orionstar A111 (calibrated using buffer solutions of pH 4.01 and 7.00). AgNP concentrations (total Ag) of 4.5 mg/L (GAH) and 9.7-10.0 mg/L, dispersed in different NaCl concentrations (from 0 to 2000 mM) and two seawaters were analysed in terms of *d* evolution over time. Appropriate quantities of concentrated AgNP solution were added to a DLS cuvette containing the solution under investigation (NaCl or seawater), mixed and immediately introduced in the instrument. The relatively high concentrations (4.5 and 9.7-10.0 mg/L) used were imposed by the minimum concentration recommended by the instrument manufacturer, which is 0.1 mg/L for a particle size of 10-100 nm.

2.3 Theoretical modeling

Colloidal particles in aqueous solution interact through attractive or repulsive forces. Those interactions depend on the surface properties of the particles, and are usually short-range in nature. The Derjaguin–Landau–Verwey–Overbeak (DLVO) theory describes the potential energy of interactions between colloids in terms of van der Waals and electric double layer interactions (Derjaguin and Landau, 1941; Gregory, 2005; Verwey et al., 1948). The balance between the additive forces determines colloidal stability. This theory has been widely applied to understand NP aggregation under different conditions (Afshinnia et al., 2017; Lin et al., 2015; Zhu et al., 2016).

Potential energy diagrams obtained from DLVO theory are useful to our understanding of colloids/NPs stability, as they can be used to predict the probability of particle aggregation. However, other forces not considered in the DLVO theory (non-DLVO forces), such as steric and hydrophobic interactions, hydration effects, or polymer bridging, can also play a key role in colloid/NP stability (Grasso et al., 2002).

The total interaction energy between two particles considering the Derjaguin integration approximation reads (Gregory, 2005):

$$V_T = -\frac{A_H}{12}\left[\frac{1}{x^2+2x} + \frac{1}{x^2+2x+1} + 2\ln\left(\frac{x^2+2x}{x^2+2x+1}\right)\right] + \pi\varepsilon\varepsilon_0 d\zeta^2 e^{(-\varkappa h)} \quad (1)$$

where A_H (J) is the Hamaker constant, $x = \frac{h}{d}$, h (nm) is the separation distance between particles, d (nm) the diameter of the particles, ε the relative permittivity, ε_0 (C/Vm) the permittivity of free space, κ (nm^{-1}) the Debye-Hückel constant and ζ (V) the zeta-potential. The first term in the right side of the equation accounts for the van der Waals attractive energy and the second for the electrical interactions. Equation 1 applies to equal spherical particles with identical zeta-potential (<50 mV), 1:1 electrolytes and for h<5 nm<< d. Although these conditions are restrictive, equation 1 is still useful as a first approximation to infer the stability of the AgNP solutions used in this study.

Upon addition of charged NPs to quiescent electrolyte solutions of different concentrations, the aggregation rates may show two distinct regimes: reaction controlled aggregation (RCA) and diffusion controlled aggregation (DCA). The former is a relatively slow aggregation regime, where the aggregation rate increases and the interaction energy barrier decreases with increasing electrolyte concentration. In contrast, in the DCA regime, the aggregation rate

is fast and constant due to the suppression of the interaction energy barrier that occurs at high electrolyte concentration.

We described the aggregation kinetics of AgNPs according to the classical Smoluchowski theory (Elimelech et al., 1995; Gregory, 2005). Aggregation is considered an irreversible second order process where the rate of collision (collision frequency) is proportional to the product of the concentrations of two identical interacting spherical particles. As not all the collisions will be successful in producing aggregates, the aggregation/collision efficiency, α, is introduced. If the initial particle concentration is the same for various electrolyte concentrations, then α can be calculated dividing the slopes of the z-average hydrodynamic diameters (*d*) *vs.* time plot in the RCA regime by the slope in the DCA regime (Kretzschmar et al., 1998):

$$\alpha = \frac{\left(\mathrm{d}d/\mathrm{d}t\right)_{t\to 0,\ \mathrm{RCA}}}{\left(\mathrm{d}d/\mathrm{d}t\right)_{t\to 0,\ \mathrm{DCA}}} \qquad (2)$$

These values of α can be regarded as "*z-averaged collision efficiencies*", to reflect the fact that they have been obtained from time-resolved DLS measurements (Gallego-Urrea et al., 2016). The use of this technique for the derivation of aggregation rates has been critically discussed in recent works (Gallego-Urrea et al., 2014). Nevertheless, from Eq. 2 it is possible to determine α without knowledge of the aggregation rate constant. In the present case, the α values were obtained at the onset of aggregation for d ≤ 2-5 d_0, where d_0 is the first value measured for the z-average hydrodynamic diameter. The values for the slopes of the *d vs t* plot used to calculate α are shown in Table S1.

247 Plotting α *versus* the electrolyte concentration allows the determination of the
248 critical coagulation concentration (CCC), as the intersection between RCA
249 and DCA regimes. The CCC represents the minimum electrolyte
250 concentration required to destabilize the NPs, and provides a simple and
251 useful stability limit of a NP suspension.
252 In the case of a fully unstable dispersion where aggregation is controlled by
253 mass transport due to Brownian diffusion (α= 1), with a constant value of the
254 absolute aggregation rate coefficient (k_a), the treatment of aggregation
255 kinetics is simplified. Theoretically, k_a only depends on the solution
256 temperature (T) and viscosity (μ) according to:
257 $$k_a = \frac{4k_B T}{3\mu} \quad (3)$$
258 where k_B is the Boltzmann constant. However, the experimentally obtained k_a
259 values (k) are usually different from the ones derived using Eq. 3 as a result of
260 hydrodynamic interactions between particles (Holthoff et al., 1996).
261 The determination of the aggregate structure is also important for the
262 establishment of the behaviour and fate of NPs. The dimensions and
263 porosities of the aggregates affect the reactivity, surface area, solubility and
264 thus toxicity of NPs (Angel et al., 2013). They also determine the effective
265 buoyant densities, which in turn regulate the gravitational settling velocities
266 (Lee et al., 2000) and, therefore, the persistence and residence time of the NP
267 aggregates in surface mixed layers of natural waters. Aggregation is usually
268 considered fractal in nature. In the DCA regime, the mass of a fractal
269 aggregate is proportional to its radius of gyration raised to a power that
270 characterizes the aggregate structure, namely the fractal dimension (D_f)
271 (Gregory, 2005). Considering the average number of primary particles

contained in an aggregate ($\bar{k}$) and assuming that the aggregate radius is proportional to the radius of gyration, the experimentally obtained hydrodynamic diameter, *d*, can be related to $\bar{k}$ using the following approximate expression:

$$d = d_0 \sqrt[D_f]{\bar{k}} = d_0 \sqrt[D_f]{1 + \alpha k N_0 t} \quad (4)$$

The initial particle number concentration, N_0 (particles/m^3), was calculated from the following formula:

$$N_0 = \frac{3}{4} \frac{C_i}{\rho \pi \left(d_i/2\right)^3} \quad (5)$$

where ρ is the Ag density (1.05×10^{-20} g/nm^3), C_i the initial AgNP concentration (4.5/9.7-10 mg/L) and d_i (nm) the z-average hydrodynamic diameter in high-purity water.

When $\alpha k N_0 t$ >>1, Eq. 4 becomes Eq. 6 and then, D_f can be obtained from the slope of the log *t*-log *d* plot in the DCA regime, according to (Lin et al., 1990):

$$d \propto t^{1/D_f} \quad (6)$$

Note that these values of D_f are empirical parameters derived from hydrodynamic diameters. It is implicitly assumed that the aggregate structure remains constant within the time window of the experiments. This is a reasonable assumption in DCA regime, where aggregation is irreversible, as the depth of the primary minimum of the interaction potential is much greater than $k_B T$, and thus restructuring of the aggregated clusters is unlikely to occur (Kim and Berg, 2000).

In addition, an experimental value for k_a (*k*) was calculated by fitting the DLS kinetic curves in the DCA regime to Eq. 4. The kinetic constants, *k*, were optimised by the nonlinear least squares minimization tool of the software

296 OriginPro 8, based on the Levenberg–Marquardt algorithm. Errors on *k*,
297 reflecting fit quality and variability in the 2–3 replicates at each NaCl
298 concentration, were used to calculate reported *k* error ranges. An alternative
299 method to determine *k* more accurately requires the use of combined static
300 and dynamic light scattering measurements (Holthoff et al., 1997).
301
302 **3. Results and discussion**
303 **3.1. Aggregation kinetics in NaCl solutions**
304 Details on the synthesis of ALG, GAL and GAH coated AgNPs, and their
305 oxidation, size and surface plasmon band (SPB) evolution over time can be
306 found in a previous paper (Lodeiro et al., 2016).
307 The studied AgNPs were stable over time in pure aqueous solution in terms of
308 aggregation and oxidation. Nevertheless, with increasing NaCl concentrations
309 and when added to natural seawaters, different behaviours were observed
310 depending on the polymer coating. The molecular weight (MW) of the
311 coatings, average Transmission Electron Microscopy (TEM) diameters, z-
312 average hydrodynamic diameter in high-purity water (d_i), Pdi and zeta-
313 potentials also measured in high-purity water are presented in Table 1.
314
315 **Table1**. *Characterization data of the AgNPs coated with: branched*
316 *Polyethylenimine (BPEI), alginate (ALG), gum arabic (GAH and GAL), tannic*
317 *acid (TA) and NM-300K in high-purity water*

	BPEI	ALG	GAH	GAL	TA	NM-300K
Coating MW*	25,000	120,000-190,000	250,000	250,000	1,701.20	n.a.

TEM (nm)	30.5 ± 2.7*	9.7 ± 0.44	n.a.	10 ± 0.29	31.2 ± 2.4*	15*
d_i (nm)	51 ± 1	48 ± 2	112 ± 9	63 ± 3	34 ± 3	48 ± 4
Pdi	0.17±0.02	0.52±0.02	0.29±0.02	0.44±0.03	0.27±0.02	0.37±0.1
zeta-potential (mV)	+56*	-70 ± 7	-43 ± 6	-41 ± 7	-39*	-4 ± 1

318 **Values provided by the manufacturer; n.a.: not available.*

319

320 The differences observed in the ratios between the NP diameters measured
321 using DLS (d_i) and TEM are attributed to differences in the coating thickness
322 and polydispersity of the NP samples. Interestingly, a linear correlation (R-
323 squared of 0.9856) was found between the diameter increase measured using
324 TEM and DLS, and the molecular weight of the coating.
325 In order to investigate the main stabilization mechanisms in the NP
326 dispersions based on the DVLO theory, potential energy diagrams were
327 obtained at different ionic strengths. Two main challenges were faced when
328 applying DVLO theory to describe the interaction forces between the AgNPs
329 in solution. First, an accurate value for the Hamaker constant (A_H) was not
330 available. Second, the fact that experimental determination of electrophoretic
331 mobilities in Ag/NaCl solutions using DLS is not straightforward (Lowry et al.,
332 2016). Precipitation of AgCl and oxidation of organic macromolecules on the
333 electrophoretic cell electrodes produces inaccurate measurements, especially
334 at high NaCl concentrations. Unfortunately, we could not find any solution to
335 solve this problem. Here we used a theoretical A_H value of 3.51×10^{-20} J as
336 obtained from Pinchuk et al. (Pinchuk, 2012). Possible modifications in the A_H
337 value as a result of different polymer coatings (size effects) were not

338 considered. Moreover, the use of zeta-potential instead of surface charge
339 values in Eq. 1 implies an additional limitation, especially for particles with
340 macromolecular coatings. The zeta-potential is not a direct measure of the
341 surface charge, but a theoretical calculation of the electrostatic potential on
342 the hydrodynamic shear (slipping plane) surrounding the particle.
343 Bearing those limitations in mind, potential energy diagrams were obtained
344 (Figure S1). The DLVO potential energy diagrams for ALG and GAH coated
345 AgNPs showed that the net energy barrier is reduced at increasing NaCl
346 concentrations, favouring AgNP aggregation. This is in accordance with our
347 aggregation experiments. In contrast, there is no energy barrier present at any
348 of the electrolyte concentrations for NM-300K AgNPs and, according to the
349 potential energy diagrams, their aggregation should be favourable regardless
350 of NaCl concentration. However, we experimentally observed a good stability
351 of NM-300K AgNPs throughout the full range of NaCl concentrations. Large
352 amounts of adsorbed polymers, e.g. Tween-20 in NM-300K NPs, can confer
353 extra stability (steric stabilization) and could explain the anomalous DLVO
354 prediction (Gregory, 2005). DLVO theory explains the aggregation process
355 qualitatively, but it does not provide quantitative information for the
356 aggregation rate constants (Afshinnia et al., 2017). Hydrodynamic interactions
357 together with the presence of macromolecular coatings adsorbed on the
358 particle surface are usually the main reasons for this inconsistency (Grasso et
359 al., 2002).
360 When AgNPs are added to NaCl solutions, the induced aggregation is
361 triggered by an increase in ionic strength that compresses the electrical
362 double layer surrounding the NPs, and also by specific electrolyte interactions

363 with the NP metallic surface and/or coating. At low NaCl concentrations (<20
364 mM), the formation of an AgCl layer is expected (Peterson et al., 2016; Zhang
365 et al., 2015). The AgCl coating passivates the NP surface and reduces its
366 charge, hindering NP oxidation. Hence, the ionic strength required to induce
367 AgNP aggregation is usually lower for NaCl than for other halide salts that do
368 not interact with the NP surface (Botasini and Méndez, 2013; Espinoza et al.,
369 2012). This fact is relevant for the study of AgNPs in seawaters, where NaCl
370 concentrations are high (e.g. 0.56 M for salinity 35).
371 The aggregation kinetics in NaCl solutions of ALG, GAL, GAH, NM-300K,
372 BPEI and TA coated AgNPs were studied using DLS (Figures 1 and S2).
373 Supply of NaCl destabilized an initially stable suspension of AgNPs, inducing
374 the formation of NP aggregates over time. We used the onset of the
375 aggregation process ($d \leq$ 2-5 d_0) to calculate D_f, α, CCC and k for the studied
376 AgNPs, when possible.
377 An increase in d over time was observed at NaCl concentrations from
378 20 (GAH), 40 (TA), 50 (ALG) and 550 (NM-300K) mM. AgNPs coated with
379 GAL and BPEI showed different behaviours. We only found a slight increase
380 of d from ~ 44 to 74 nm for AgNP-GAL at [NaCl]= 997 mM after 50 min. For
381 AgNP-BPEI no noticeable aggregation was observed over the time window
382 studied (~1 h) at NaCl concentrations up to 997 mM. Moreover, a decrease of
383 the z-average hydrodynamic diameters at low NaCl concentrations was
384 observed for some of the coatings, when compared to the values found in
385 high-purity water (Figures 1 and S2). As mentioned above, our hypothesis is
386 that interactions of NaCl with the surface and coating of the NPs may play a
387 key role due to the increase in the ionic strength and/or specific electrolyte

388 interactions. Accordingly, the observed trend for this decrease in the z-
389 average hydrodynamic diameters is the following: GAH>GAL>TA>ALG>NM-
390 300K≈BPEI. This trend is in accordance with our hypothesis: for large neutral
391 organic coatings (e.g. NM-300K) or highly charged stable polymers (e.g.
392 BPEI) no significant differences were observed between *d* values in high-
393 purity water and NaCl at low concentrations. On the contrary, the weakest
394 electrostatic stabilized coatings (e.g. GA and TA) show the largest differences
395 in the z-average hydrodynamic diameters in NaCl compared to high-purity
396 water.
397 Besides, several of the obtained aggregation kinetic profiles showed a slight
398 to moderate decrease in *d* at the very beginning of aggregation (20-30 s after
399 mixing), compared to the values obtained in high-purity water (Figure S3).
400 This phenomenon is not unprecedented. In fact, the formation of new NPs (Ag
401 or AgCl NPs) from silver species reduction and AgCl precipitation has been
402 reported to lead to apparent average smaller sizes of NPs at initial stages
403 (Baalousha et al., 2013b). Accordingly, a reduction in the surface plasmon
404 resonance band area was also observed at the onset of aggregation for ALG
405 and GAH coated AgNPs measured by UV-visible spectrophotometry (Lodeiro
406 et al., 2016). Moreover, this decrease in *d* values can be also ascribed to
407 partial dissolution of AgNPs or disruption of the chemical equilibrium of the
408 coatings.
409 The aggregation kinetic data obtained by DLS should be interpreted with
410 caution. As mentioned before, DLS observations might include not only
411 responses of AgNPs originally present in solution, but also the possible
412 formation of concomitant (nano)particles of AgCl or even new AgNPs (by

413 reduction of residual Ag^+ ions present in the stock dispersion), making data
414 interpretation more challenging. Moreover, the cumulant analysis used to
415 obtain the *d* values is only recommended for spherical, narrowly distributed
416 and monodisperse systems.
417 The aggregation z-averaged collision efficiencies, α, for GAH, TA, ALG and
418 NM-300K coated AgNPs in NaCl solutions were calculated using Eq. 2. The
419 CCC values (Table 2) indicated that NM-300K was more stable than GAH, TA
420 or ALG coated AgNPs in NaCl solutions (Figure 1). The enhanced stability is
421 attributed to the stronger steric interaction provided by the non-ionic NM-300K
422 coating. The presence of residual Ag^+ ions in the GAH AgNP stock solution
423 influences its aggregation behaviour.
424 In fact, the GAH AgNP solutions displayed a non-monotonic trend of
425 aggregation rate with NaCl concentration: at high NaCl concentrations (≥ 343
426 mM) the DLS data showed constant *d* values (Figure 1a). The concentration
427 of the silver ions/species in the measured GAH NP solutions was $\sim 1.6\times10^{-5}$ M,
428 higher than the solubility product of AgCl at $[Cl^-]$> 22 μM. Therefore, some
429 contribution from AgCl precipitation, probably modifying the NP
430 surface/coating, is expected. The stability of ALG AgNPs showed a
431 contribution from electrostatic repulsion due to deprotonation of the
432 carboxylate groups present in alginate at pH 8 (Rey-Castro et al., 2004).
433 Accordingly, we measured only a relatively slight decrease in zeta-potential
434 (from -70 to -40 mV) with increasing NaCl concentrations (from 0 to 85 mM).
435 Some steric effect from the ALG coating is also anticipated. However, it is not
436 unlikely that electrostatic interactions prevail over steric stabilization in the

case of the TA coating due to the weak acidity of tannic acid, pK~8.2 (Cruz et al., 2000) that provides a zeta-potential of -39.1 mV in high-purity water.

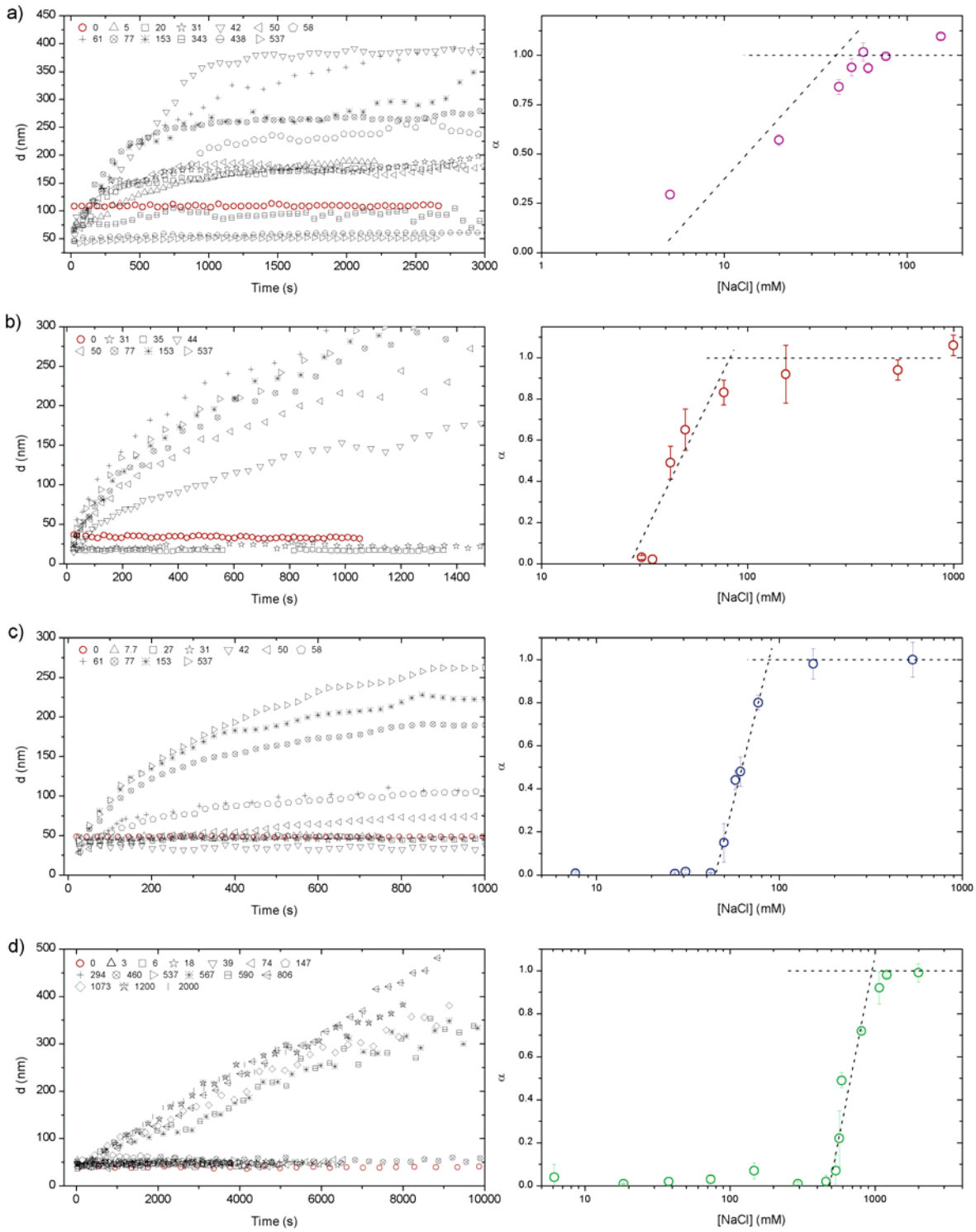

Figure 1. Left panel: Evolution of the z-average hydrodynamic diameter (*d*) over time in aqueous solution at pH 8.0 measured by DLS at increasing NaCl

462 concentrations (mM) for: a) GAH : b) TA; c) ALG and d) NM-300K coated
463 AgNPs at concentrations of 4.5 (GAH) and 9.7-10 mg/L (TA, ALG and NM-
464 300K) Aggregation of these AgNPs was observed at NaCl concentrations
465 from 20 (GAH), 40 (TA), 50 (ALG) and 550 (NM-300K) mM Right panel:
466 Values of α obtained from the slopes of straight lines fitted to the data ($d \leq$ 2-5
467 d_0) presented in the left panel. The intersection between the RCA and DCA
468 regimes (dashed lines) provides the CCC values, used as stability limit for the
469 AgNP suspensions.
470
471 Interestingly, the polysaccharides ALG and GA somehow seem to provide a
472 weaker steric hindrance to aggregation in ALG/GAH coated AgNPs than the
473 synthetic non-ionic surfactants in NM-300K.
474 On the other hand, BPEI AgNPs, which are the only positively charged NPs
475 examined in the current study, remained stable in NaCl solutions up to 997
476 mM and in this case, both steric and electrostatic stabilization are expected.
477 For most of the coatings, the NP aggregation behaviours were comparable
478 between DLS or UV-visible spectrophotometry techniques. For example, the
479 CCC values shown in this work are in agreement with those previously
480 obtained for ALG (80 mM) and GAH (45 mM) coated AgNPs at the same NP
481 concentration (Lodeiro et al., 2016). A good agreement was also found
482 between DLS and UV-visible measurements for AgNP-GAL. At NaCl
483 concentrations <153 mM and experimental durations shorter than 1000 s, the
484 plasmon resonance band (PRB) area and *d* showed very small changes.
485 In contrast, DLS measurements showed slightly higher stabilities of the
486 AgNPs (lower α values) at low NaCl concentrations. Moreover, results

observed for GAH AgNP aggregation kinetics by UV-visible measurements indicated a higher stability of GAH AgNPs in solution than in the DLS measurements conducted over longer time periods (>1 h). The constant *d* values observed at NaCl concentrations ≥ 343 mM using DLS were also reflected in the PRB area observations, which indicated an approximate 12% decrease within an equivalent time window (Lodeiro et al., 2016).

The packing density of the aggregates in the DCA regime was calculated using Eq. 6. If the collision efficiency is low (RCA regime) Eq. 6 is no longer valid, and D_f should be obtained by static light scattering or transmission electron microscopy measurements (Baalousha et al., 2008; He et al., 2013). The obtained D_f values (Table 2) are in agreement with those expected from colloid aggregation theory, ~1.7-1.8 (Lin et al., 1990; Zhang, 2014) and also with the estimated values from other studies using different AgNPs (Bertrand et al., 2016; He et al., 2013).

Table 2. *Critical coagulation concentration (CCC) values obtained from Eq. 2 at different NaCl concentrations. Fractal dimension (D_f) values obtained from Eq. 6, experimental aggregation rate constants (k) obtained from Eq. 4, both on the DCA regime, and initial particle number concentration* (N_0). *Data and fits are presented in Figures 1 (CCC), S4 (D_f) and 2 (k)*

AgNP coating	CCC (mM)	D_f	k ($m^3 \cdot s^{-1}$) $\times 10^{18}$	N_0 (NP/m^3) $\times 10^{-16}$
GAH	41 ± 7.2	2.0 ± 0.3[1] / 1.99 ± 0.04[2]	2.9±0.6	0.49
TA	82 ± 5.0	1.73 ± 0.09[4] / 1.78±0.08[5]	1.1±0.2	4.63
ALG	84 ± 2.2	1.8 ± 0.1[3] / 1.70 ± 0.08[4]	2.2±0.2	1.60

NM-300K	986 ± 100	1.81±0.03[6] / 1.86±0.07[7]	0.15±0.03	1.65
BPEI	n.a.	n.a.	n.a.	–
GAL	n.a.	n.a.	n.a.	–

[NaCl]= 50[1], 58[2], 153[3], 537[4], 997[5], 1200[6] and 2000[7] mM; n.a.: not available (the dispersions were stable throughout the range of NaCl concentrations studied)

The obtained aggregation curves in the DCA regime were fitted to Eq. 3 to estimate the experimental values of the absolute aggregation constant, *k*, (Figure 2). The required D_f values were obtained using Eq. 6 (Table 2).

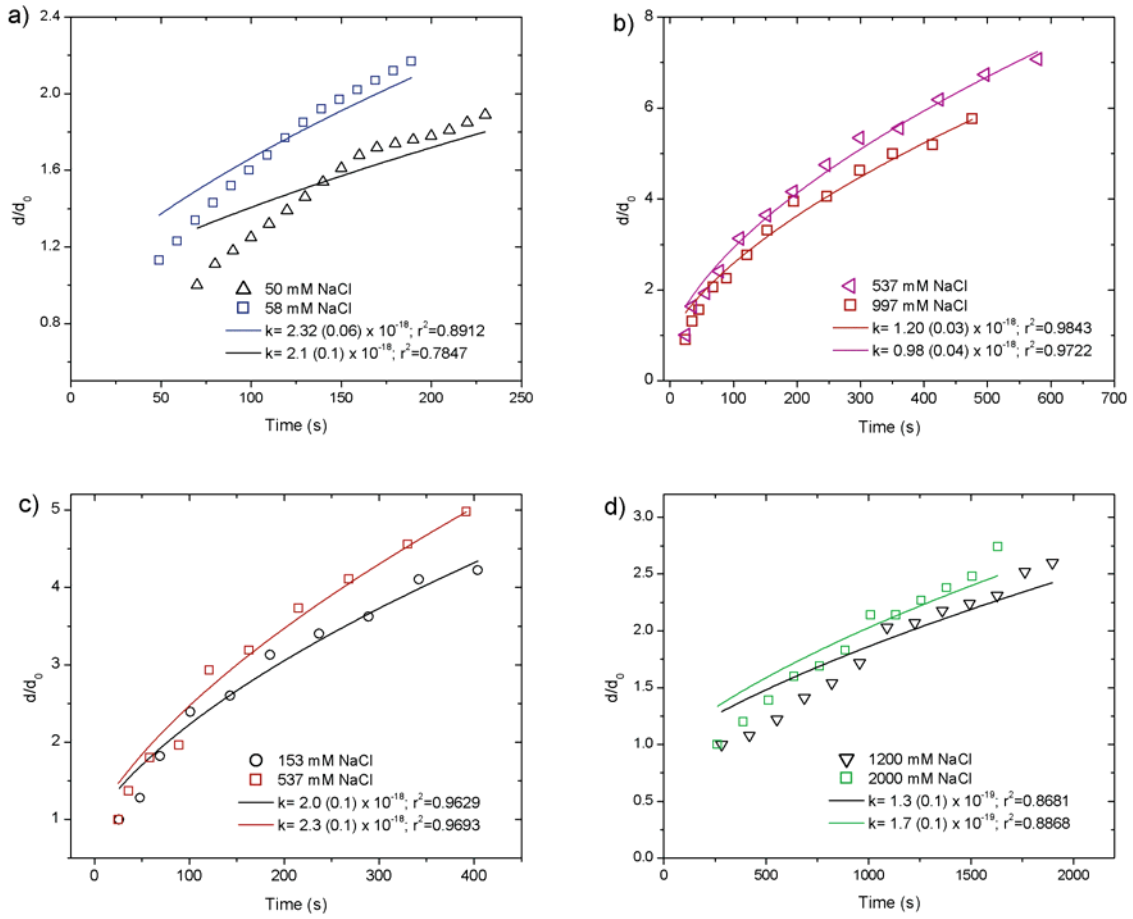

Figure 2. Aggregation kinetics in the diffusion controlled aggregation (DCA) regime for : a) GAH; b) TA; c) ALG and d) NM-300K coated AgNPs. The lines represent the fit of the corresponding aggregation kinetics using Eq. 4, where

529 *k* was used as the only fitting parameter. The numbers between parentheses
530 represent the fitting error. The obtained aggregation rate constants for GAH
531 and ALG coated AgNPs were of the same order of magnitude as the
532 theoretical k_a value, while for TA and NM-300K *k* values were one order of
533 magnitude lower.
534
535 Experimental aggregation rate constants were usually 2-4 fold lower than the
536 expected theoretical k_a value (6.1×10^{-18} $m^3 \cdot s^{-1}$ in a 550 mM NaCl solution)
537 (Holthoff et al., 1997). In agreement, our results for GAH and ALG coated
538 AgNPs showed aggregation rate constants ~2-5 fold smaller than k_a (Table 2).
539 In contrast, the experimental *k* value obtained for NM-300K coated AgNPs
540 was considerably lower (Table 2). The errors show the standard deviation
541 between two measurements undertaken on the DCA regime (Figure 2), where
542 the *k* values should not change with NaCl concentration. The discrepancies in
543 the obtained *k* values can be explained by hydrodynamic and/or counterion-
544 specific interactions (Gregory, 2005). Moreover, the uncertainty in the initial
545 size and particle number concentration calculations results in approximate *k*
546 values. It would be important for future studies to compare the values
547 obtained in this work using Equations 4 and 6 with those provided by static
548 and dynamic light scattering measurements, which would allow a significant
549 improvement in the reliability of experimental *k* values (Holthoff et al., 1996).
550
551 **3.2. Aggregation kinetics in natural seawaters**
552 We also conducted aggregation studies in seawaters from a Baltic fjord and
553 an Atlantic coastal area in northwest Spain, which were compared with the

554 results of NaCl experiments. A detailed analysis of the seawater samples is
555 provided in the electronic supplementary information (Table S2). The
556 calculated ionic strength (*I*) values (Table S2) in the Baltic fjord (346 mM) and
557 the Spanish coastal (706 mM) seawaters were higher than the CCC values
558 obtained in NaCl solutions (where *I* is equal to concentration) for TA and ALG
559 coated AgNPs (Table 2). For GAH, even if the obtained CCC value was
560 considerably lower than *I* in the seawaters studied, a constant *d* value was
561 observed at [NaCl] ≥ 343 mM. Therefore, if AgNP behaviour is mainly
562 controlled by the ionic strength, a similar aggregation rate is expected at
563 equivalent ionic strength once AgNPs were added to the natural seawaters.
564 Remarkably, and opposite to what we observed in NaCl solutions, d_0 values in
565 seawater were somewhat larger than those obtained in high-purity water for
566 the studied coatings, except GA and TA coated AgNPs in Baltic fjord
567 seawater (Figure S3). We hypothesize that the presence of organic matter in
568 the seawater solutions influenced the DLS measurements and produced the
569 increase in d_0 values.
570 The aggregation stability of each NP batch in NaCl and seawater media was
571 compared on the basis of interpolated collision z-averaged collision
572 efficiencies (α_i) for NaCl concentrations of ionic strength comparable with that
573 of the seawater samples (346 and 706 mM). The collision efficiency in
574 seawater (α_{SW}) was approximated as:

575 $$\alpha_{sw} = \frac{\left({}^{dd}/_{dt}\right)_{t\to 0,\ seawater}}{\left({}^{dd}/_{dt}\right)_{t\to 0,\ DCA(NaCl)}} \quad (7)$$

576 Finally, both α_{SW} and $\alpha_{\square}$ values were compared through a t-test. The $\alpha_{\square}$
577 values were obtained for TA, ALG and NM-300K coated AgNPs (Table S4).

578 The BPEI and GAL coatings were stable throughout the range of NaCl
579 concentrations studied, while the GAH coating presented a non-monotonic
580 aggregation rate. Therefore, the interpolation of the z-averaged collision
581 efficiencies was not possible in these cases.
582 The GAH NPs displayed an intermediate behaviour between low (153 mM)
583 and high (343-537 mM) NaCl concentrations when added to the natural
584 seawaters (Figure 3a), while the TA coated AgNPs showed very similar
585 aggregation rates in the Baltic fjord (*I*= 346 mM) and in NaCl 153 and 537 mM
586 (Figure 3b). In contrast, the ALG AgNPs were more stable in the seawaters
587 studied than in NaCl solutions at equivalent ionic strengths (Figure 3c). Some
588 of the AgNPs that were stable in NaCl solutions (GAL and NM-300K coated
589 NPs) showed no significant aggregation in either the Baltic or the Spanish
590 coastal seawaters during the time window studied. Moreover, at high ionic
591 strengths ($I \geq 588$ mM) both GAL and NM-300K AgNPs showed somewhat
592 lower sizes in seawater than in NaCl solution (Figure 3d,e). On the other
593 hand, BPEI AgNPs, which have a positively charged coating, showed a fast
594 aggregation rate in the seawaters (Figure 3f), opposite to the stable behaviour
595 observed in NaCl solutions at 997 mM ionic strength (Figure S2a). From the
596 obtained results we can deduce that strongly steric-stabilized AgNPs (NM-
597 300K and GAL) are stable in both NaCl solutions and natural seawaters within
598 the studied range of salinities (17.19-34.65) and organic content (277-83.67
599 μM DOC). For electrostatically stabilized NPs, the absolute value of their
600 charge and its sign played an important role; when electrostatic stabilization
601 was high (ALG), the NPs showed slower aggregation in the natural seawaters
602 studied compared to NaCl solutions at equivalent ionic strength.

Nevertheless, if weakly electrostatically stabilized NPs were used (GAH and TA coated AgNPs), fast aggregation was observed in both solutions.

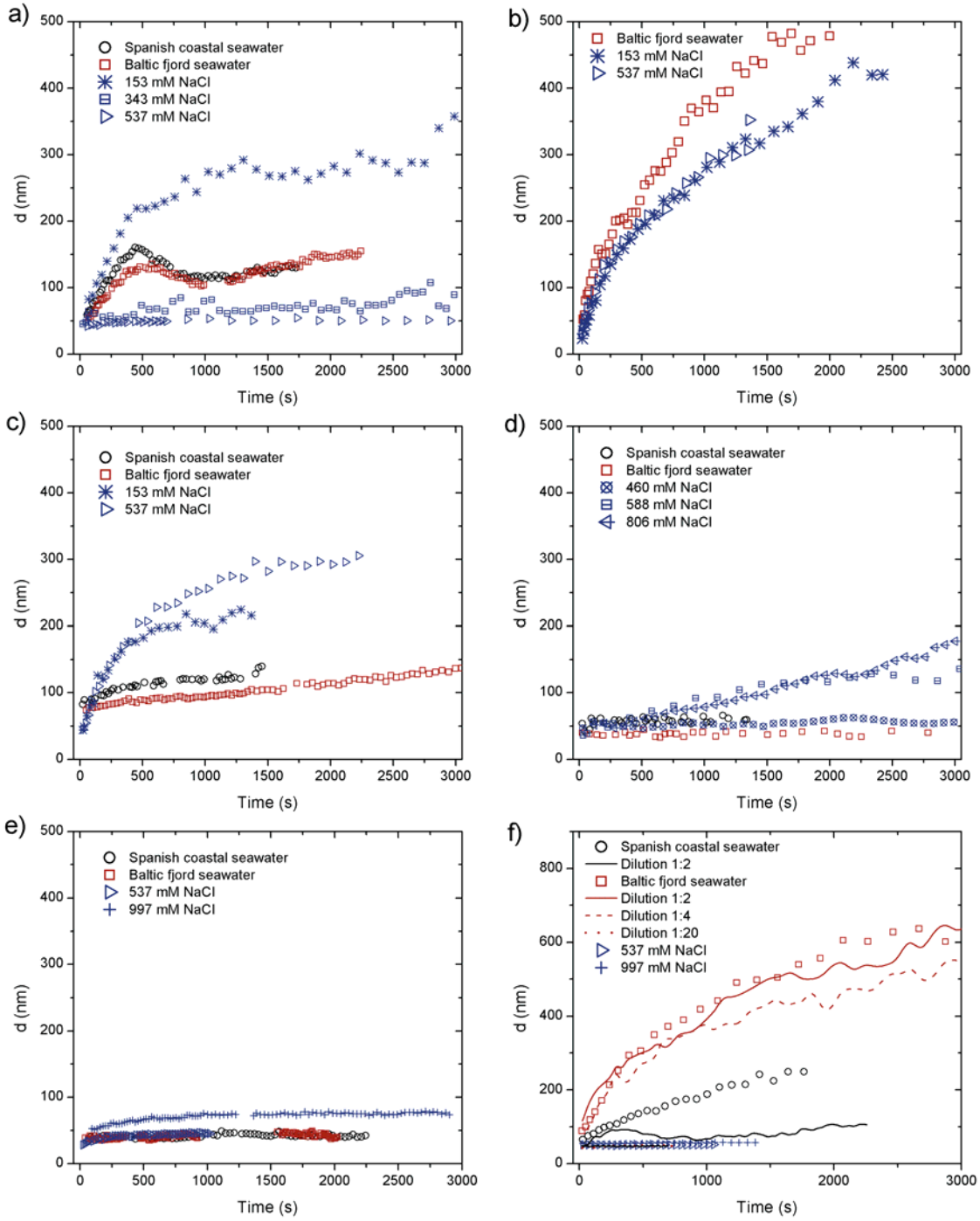

Figure 3. Aggregation kinetics in Baltic fjord and Spanish coastal seawaters for: a) GAH, b) TA, c) ALG, d) NM-300K, e) GAL and f) BPEI coated AgNPs. The strongly steric-stabilized AgNPs (NM-300K and GAL) are stable in both

NaCl solutions and natural seawaters. The strongly electrostatically stabilized AgNPs (ALG) showed slower aggregation in the natural seawaters, while the weakly electrostatically stabilized NPs (GAH and TA) showed a fast aggregation in both solutions. The positively charged BPEI AgNPs are stable in NaCl solutions but not in seawater.

Surprisingly, BPEI AgNPs, a strongly electro-steric stabilized NP that is very stable in highly concentrated NaCl solutions, showed rapid aggregation after addition to seawaters, probably determined by its positively charged coating and the subsequent partial neutralization by the oppositely charged DOM in seawater. Dilution of Baltic fjord seawater with high-purity water progressively reduced the aggregation kinetic factor. When the dilution was 1:20, a constant *d* value was observed over time (Figure 3f). Dilution of Spanish coastal seawater also stabilized the BPEI AgNP solution. The dilution effect was more pronounced, and a 1:2 dilution was sufficient to significantly decrease the aggregation of the NPs, indicating dependence of the stabilization effect on the AgNP/DOM ratio.

This study illustrates that extrapolation of NP aggregation results obtained in synthetic solutions (e.g. NaCl) to natural seawaters is challenging. Hence, more research efforts are needed to investigate the role of other inorganic (major divalent cations and anions) and organic (DOM) components of the seawater matrix in stabilizing polymer-coated NPs. To do so, isolation and characterization of marine DOM, which represents a major endeavour, is required. The interactions of DOM with the coated NPs may presumably lead to the formation of complex ecocoronas (biomolecule shell), involving several

processes such as ligand exchange with coating polymers (preferential adsorption), bridging, electrostatic and/or steric stabilization mechanisms, etc. All these interactions should be taken into account when describing the aggregation process. Moreover, cautious extrapolation to very low NP concentrations of environmental relevance (ppt range) is advised, given the estimated theoretical background concentrations reported in literature as a result of diffuse NP contamination sources.

4. Conclusions

The z-averaged collision efficiencies, effective aggregation rates and fractal structures have been obtained in NaCl for the GAH, TA, ALG and NM-300K AgNP batches, whereas BPEI and GAL dispersions were practically stable up to *ca*. 1M NaCl. Only some of these nanomaterials (TA, NM-300K, GAL) have similar aggregation rates in seawater samples and NaCl solutions of comparable ionic strength.

In the cases of TA (and possibly ALG AgNPs in seawaters with very low DOM contents), aggregation and subsequent settling are, presumably, the more relevant fates (even in absence of heteroaggregation processes with natural particulate matter). On the other hand, NM-300K and GAL AgNPs are expected to be very stable and persistent/mobile in seawater (and thus potentially more available for uptake by marine biota). The AgNPs coated with BPEI and GAH showed complex behaviours in the seawater samples that are definitely not predicted using simple NaCl solutions, where BPEI coating seems to be affected by charge neutralization due to surface adsorption of marine DOM.

678

679 **Supplementary material**

680 Tables S1-S4 and Figures S1-S4.

681

682 **Data statement**

683 The datasets generated during and/or analysed during the current study are

684 available from the corresponding author on reasonable request.

685

686 **Acknowledgements**

687 This research was supported by a Marie Curie Intra European Fellowship

688 within the 7th European Community Framework Programme [grant agreement

689 number PIEF-GA-2012-329575]. CRC acknowledges support from FEDER

690 and the Spanish Ministry of Education and Science [Project No. CTM2016-

691 78798], and from European Union Seventh Framework Programme FP7-

692 NMP.2012.1.3-3 [grant agreement no. 310584] (NANoREG).

693

694 **References**

695 Afshinnia K, Marrone B, Baalousha M. Potential impact of natural organic

696 ligands on the colloidal stability of silver nanoparticles. Science of The

697 Total Environment 2018; 625: 1518-1526.

698 Afshinnia K, Sikder M, Cai B, Baalousha M. Effect of nanomaterial and media

699 physicochemical properties on Ag NM aggregation kinetics. Journal of

700 Colloid and Interface Science 2017; 487: 192-200.

701 Angel BM, Batley GE, Jarolimek CV, Rogers NJ. The impact of size on the
702 fate and toxicity of nanoparticulate silver in aquatic systems.
703 Chemosphere 2013; 93: 359-365.
704 Arvidsson R, Molander S, Sanden BA, Hassellov M. Challenges in Exposure
705 Modeling of Nanoparticles in Aquatic Environments. Human and
706 Ecological Risk Assessment 2011; 17: 245-262.
707 Baalousha M, Manciulea A, Cumberland S, Kendall K, Lead JR. Aggregation
708 and surface properties of iron oxide nanoparticles: Influence of pH and
709 natural organic matter. Environmental Toxicology and Chemistry 2008;
710 27: 1875-1882.
711 Baalousha M, Nur Y, Romer I, Tejamaya M, Lead JR. Effect of monovalent
712 and divalent cations, anions and fulvic acid on aggregation of citrate-
713 coated silver nanoparticles. Science of the Total Environment 2013a;
714 454: 119-131.
715 Baalousha M, Nur Y, Römer I, Tejamaya M, Lead JR. Effect of monovalent
716 and divalent cations, anions and fulvic acid on aggregation of citrate-
717 coated silver nanoparticles. Science of the Total Environment 2013b;
718 454–455: 119-131.
719 Bertrand C, Zalouk-Vergnoux A, Giambérini L, Poirier L, Devin S, Labille J, et
720 al. The influence of salinity on the fate and behavior of silver
721 standardized nanomaterial and toxicity effects in the estuarine bivalve
722 Scrobicularia plana. Environmental Toxicology and Chemistry 2016;
723 35: 2550-2561.

724 Botasini S, Méndez E. Silver nanoparticle aggregation not triggered by an
725 ionic strength mechanism. Journal of Nanoparticle Research 2013; 15:
726 1526.
727 Bour A, Mouchet F, Silvestre J, Gauthier L, Pinelli E. Environmentally relevant
728 approaches to assess nanoparticles ecotoxicity: A review. Journal of
729 Hazardous Materials 2015; 283: 764-777.
730 Brar SK, Verma M. Measurement of nanoparticles by light-scattering
731 techniques. TrAC-Trends in Analytical Chemistry 2011; 30: 4-17.
732 Chekli L, Zhao YX, Tijing LD, Phuntsho S, Donner E, Lombi E, et al.
733 Aggregation behaviour of engineered nanoparticles in natural waters:
734 Characterising aggregate structure using on-line laser light scattering.
735 Journal of Hazardous Materials 2015; 284: 190-200.
736 Chernousova S, Epple M. Silver as Antibacterial Agent: Ion, Nanoparticle, and
737 Metal. Angewandte Chemie International Edition 2013; 52: 1636-1653.
738 Cruz BH, Díaz-Cruz JM, Ariño C, Esteban M. Heavy Metal Binding by Tannic
739 Acid: A Voltammetric Study. Electroanalysis 2000; 12: 1130-1137.
740 Dale AL, Lowry GV, Casman EA. Accurate and fast numerical algorithms for
741 tracking particle size distributions during nanoparticle aggregation and
742 dissolution. Environmental Science: Nano 2017; 4: 89-104.
743 Derjaguin BV, Landau L. Theory of the stability of strongly charged lyophobic
744 sols and of the adhesion of strongly charged particles in solutions of
745 electrolytes. Acta Phys. Chim. URSS 1941; 14: 633-662.
746 Elimelech M, Gregory J, Jia X, Williams RA. Particle deposition and
747 aggregation : measurement, modelling, and simulation. Oxford England
748 ; Boston: Butterworth-Heinemann, 1995.

749 Ellis LJA, Valsami-Jones E, Lead JR, Baalousha M. Impact of surface coating
750 and environmental conditions on the fate and transport of silver
751 nanoparticles in the aquatic environment. Science of the Total
752 Environment 2016; 568: 95-106.
753 Espinoza MG, Hinks ML, Mendoza AM, Pullman DP, Peterson KI. Kinetics of
754 Halide-Induced Decomposition and Aggregation of Silver
755 Nanoparticles. The Journal of Physical Chemistry C 2012; 116: 8305-
756 8313.
757 Gallego-Urrea JA, Hammes J, Cornelis G, Hassellov M. Coagulation and
758 sedimentation of gold nanoparticles and illite in model natural waters:
759 Influence of initial particle concentration. Nanoimpact 2016; 3-4: 67-74.
760 Gallego-Urrea JA, Perez Holmberg J, Hassellöv M. Influence of different types
761 of natural organic matter on titania nanoparticle stability: effects of
762 counter ion concentration and pH. Environ. Sci.: Nano 2014; 1: 181-
763 189.
764 Grasso D, Subramaniam K, Butkus M, Strevett K, Bergendahl J. A review of
765 non-DLVO interactions in environmental colloidal systems. Reviews in
766 Environmental Science and Biotechnology 2002; 1: 17-38.
767 Gregory J. Particles in Water: Properties and Processes: CRC Press, 2005.
768 Handy RD, von der Kammer F, Lead JR, Hassellöv M, Owen R, Crane M. The
769 ecotoxicology and chemistry of manufactured nanoparticles.
770 Ecotoxicology 2008; 17: 287-314.
771 He D, Bligh MW, Waite TD. Effects of Aggregate Structure on the Dissolution
772 Kinetics of Citrate-Stabilized Silver Nanoparticles. Environmental
773 Science & Technology 2013; 47: 9148-9156.

774 Holthoff H, Egelhaaf SU, Borkovec M, Schurtenberger P, Sticher H.
775 Coagulation Rate Measurements of Colloidal Particles by
776 Simultaneous Static and Dynamic Light Scattering. Langmuir 1996; 12:
777 5541-5549.
778 Holthoff H, Schmitt A, Fernández-Barbero A, Borkovec M, Cabrerízo-Vílchez
779 Má, Schurtenberger P, et al. Measurement of Absolute Coagulation
780 Rate Constants for Colloidal Particles: Comparison of Single and
781 Multiparticle Light Scattering Techniques. Journal of Colloid and
782 Interface Science 1997; 192: 463-470.
783 Kim AY, Berg JC. Fractal aggregation: Scaling of fractal dimension with
784 stability ratio. Langmuir 2000; 16: 2101-2104.
785 Klein CL, Comero S, Locoro G, Gawllk BM, Stahlmecke B, Romazanov J, et
786 al. NM-Series of representative manufactured nanomaterials. NM-300
787 silver characterisation, stability, homogeneity - Study. EUR – Scientific
788 and Technical Research series. European Commission. Joint
789 Research Centre. Institute for Health and Consumer Protection,
790 Luxembourg, 2011, pp. 84.
791 Kretzschmar R, Holthoff H, Sticher H. Influence of pH and humic acid on
792 coagulation kinetics of kaolinite: A dynamic light scattering study.
793 Journal of Colloid and Interface Science 1998; 202: 95-103.
794 Lee DG, Bonner JS, Garton LS, Ernest ANS, Autenrieth RL. Modeling
795 coagulation kinetics incorporating fractal theories: a fractal rectilinear
796 approach. Water Research 2000; 34: 1987-2000.

797 Lin D, Ma S, Zhou K, Wu F, Yang K. The effect of water chemistry on
798 homoaggregations of various nanoparticles: Specific role of Cl- ions.
799 Journal of Colloid and Interface Science 2015; 450: 272-278.
800 Lin MY, Lindsay HM, Weitz DA, Klein R, Ball RC, Meakin P. Universal
801 diffusion-limited colloid aggregation. Journal of Physics: Condensed
802 Matter 1990; 2: 3093.
803 Lodeiro P, Achterberg EP, El-Shahawi MS. Detection of silver nanoparticles in
804 seawater at ppb levels using UV–visible spectrophotometry with long
805 path cells. Talanta 2017; 164: 257-260.
806 Lodeiro P, Achterberg EP, Pampín J, Affatati A, El-Shahawi MS. Silver
807 nanoparticles coated with natural polysaccharides as models to study
808 AgNP aggregation kinetics using UV-Visible spectrophotometry upon
809 discharge in complex environments. Science of the Total Environment
810 2016; 539: 7-16.
811 Lowry GV, Hill RJ, Harper S, Rawle AF, Hendren CO, Klaessig F, et al.
812 Guidance to improve the scientific value of zeta-potential
813 measurements in nanoEHS. Environmental Science: Nano 2016; 3:
814 953-965.
815 Massarsky A, Trudeau VL, Moon TW. Predicting the environmental impact of
816 nanosilver. Environmental Toxicology and Pharmacology 2014; 38:
817 861-873.
818 McGillicuddy E, Murray I, Kavanagh S, Morrison L, Fogarty A, Cormican M, et
819 al. Silver nanoparticles in the environment: Sources, detection and
820 ecotoxicology. Science of The Total Environment 2017; 575: 231-246.

821 Metreveli G, Frombold B, Seitz F, Grun A, Philippe A, Rosenfeldt RR, et al.
822 Impact of chemical composition of ecotoxicological test media on the
823 stability and aggregation status of silver nanoparticles. Environmental
824 Science: Nano 2016; 3: 418-433.
825 Nowack B, Krug HF, Height M. 120 Years of Nanosilver History: Implications
826 for Policy Makers. Environmental Science & Technology 2011; 45:
827 1177-1183.
828 Ohshima H. Theory of Colloid and Interfacial Electric Phenomena. In: Hiroyuki
829 O, editor. Interface Science and Technology. Volume 12. Elsevier,
830 2006, pp. v-vi.
831 Peterson KI, Lipnick ME, Mejia LA, Pullman DP. Temperature Dependence
832 and Mechanism of Chloride-Induced Aggregation of Silver
833 Nanoparticles. The Journal of Physical Chemistry C 2016; 120: 23268-
834 23275.
835 Pinchuk AO. Size-Dependent Hamaker Constant for Silver Nanoparticles. The
836 Journal of Physical Chemistry C 2012; 116: 20099-20102.
837 Pokhrel LR, Dubey B, Scheuerman PR. Natural water chemistry (dissolved
838 organic carbon, pH, and hardness) modulates colloidal stability,
839 dissolution, and antimicrobial activity of citrate functionalized silver
840 nanoparticles. Environmental Science: Nano 2014; 1: 45-54.
841 Praetorius A, Scheringer M, Hungerbühler K. Development of Environmental
842 Fate Models for Engineered Nanoparticles—A Case Study of TiO2
843 Nanoparticles in the Rhine River. Environmental Science & Technology
844 2012; 46: 6705-6713.

Quik JTK, van De Meent D, Koelmans AA. Simplifying modeling of nanoparticle aggregation–sedimentation behavior in environmental systems: A theoretical analysis. Water Research 2014; 62: 193-201.

Rey-Castro C, Herrero R, Sastre de Vicente ME. Gibbs-Donnan and specific ion interaction theory descriptions of the effect of ionic strength on proton dissociation of alginic acid. Journal of Electroanalytical Chemistry 2004; 564: 223-230.

Scheringer M, Praetorius A, Goldberg ES. Environmental Fate and Exposure Modeling of Nanomaterials. Frontiers of Nanoscience 2014; 7: 89-125.

Sharma VK. Stability and Toxicity of Silver Nanoparticles in Aquatic Environment: A Review. Sustainable Nanotechnology and the Environment: Advances and Achievements. 1124. American Chemical Society, 2013, pp. 165-179.

Tantra R, Bouwmeester H, Bolea E, Rey-Castro C, David CA, Dogné J-M, et al. Suitability of analytical methods to measure solubility for the purpose of nanoregulation. Nanotoxicology 2016; 10: 173-184.

Verwey E, Overbeek J, van Nes K. The theory of the stability of liophobic colloids: The interaction of sol particles having an electric double layer. Amsterdam: Elsevier, 1948.

Zhang L, Li X, He R, Wu L, Zhang L, Zeng J. Chloride-induced shape transformation of silver nanoparticles in a water environment. Environmental Pollution 2015; 204: 145-151.

Zhang W. Nanoparticle Aggregation: Principles and Modeling. In: Capco DG, Chen Y, editors. Nanomaterial: Impacts on Cell Biology and Medicine. Springer Netherlands, Dordrecht, 2014, pp. 19-43.

870 Zhu T, Lawler DF, Chen Y, Lau BLT. Effects of natural organic matter and
871 sulfidation on the flocculation and filtration of silver nanoparticles.
872 Environmental Science: Nano 2016; 3: 1436-1446.
873